International Journal of Fatigue 148 (2021) 106221

Contents lists available at ScienceDirect

International Journal of Fatigue

journal homepage: www.elsevier.com/locate/ijfatigue

A segmented load spectrum model for high-speed trains and its inflection stress as an indicator for line quality

Zheng Yuan [a], Xianjia Chen [b], Lijun Ma [a,c], Qiang Li [a,*], Shouguang Sun [a], Yujie Wei [b,*]

[a] School of Mechanical, Electronic and Control Engineering, Beijing Jiaotong University, Beijing 100044, China
[b] LNM, Institute of Mechanics, Chinese Academy of Sciences, Beijing 100190, China
[c] CRRC Qingdao Sifang Co., Ltd, Qingdao 266111, China

ARTICLE INFO

Keywords:
Load spectrum
Segmented Weibull distribution
Bogie frame
High-speed train
Inflection stress

ABSTRACT

Load spectrum plays a pivotal role for fault diagnosis and reliability evaluation. Here we performed long-term field tests to investigate the characteristics of load spectra of the bogie frame in a high-speed train. With increasing steps of classifications, we reveal an apparent segmented feature of the load spectrum. We propose a new theoretical model, a segmented Weibull distribution, to describe this new characteristic. Contrast to existing models, the inflection stress in our segmented Weibull model can be employed to describe the quality of lines, and the directly parameterization for the load spectrum - line quality relationship is hardly seen in existing literature. These findings reported here are in generally applicable to other dynamic systems where fatigue failure is of paramount importance.

1. Introduction

Load spectrum has been broadly employed to assess the reliability of individual components in complex engineering systems, where preexisting short cracks or newly initiated tiny ones from defects or inclusions may grow to a critical length beyond which is doomed to catastrophic failure by fast fracture. In practice, the load has various forms, such as force, stress, strain, acceleration, and so forth, and the spectrum of the particular load type, in turn, is termed as force spectrum, stress spectrum, strain spectrum, and acceleration spectrum. Since the stress spectrum from structural monitoring could be directly used for fatigue analyses [1], other types of load spectra may be used as inputs in modelling and simulations, e.g., finite element calculations, whose outputs are then used for failure analysis [2]. So far, many principles and methods for data collection, processing and analyses, and load spectrum compilation have been developed [3–5]. Recent researches on load spectrum have focused on the development of spectrum compilation methods [6] and its application in structural fatigue analysis [7]. Simplified load spectra, such as the truncated load spectrum [8], three step-up acceleration load spectrum [9] and so forth, are employed to fatigue tests of materials and structures.

Ever-increasing operating speed and prolonged operating distance have led to more diverse and harsh service conditions for high-speed trains (HSTs). While many components and parts of a HST may face the risks of fatigue failure, the bogie frames, devices between wheelsets and the car bodies, are one of the most pivotal load-bearing and load-transmission components of a HST. The state of a bogie frame will directly affect the safety and stability of trains. However, the bogie frame often suffer from fatigue in service, which may endanger the safety of the whole rail [10–12]. Regarding the fatigue design of railway vehicle structures, although international technical standards such as EN (European Standard) and UIC (International Union of Railways) provide general guidance, there is a grand challenge to implement those specifications to components of a HST under different line conditions [13,14]. Field tests enable us acquire vast amounts of load-time historical data from monitoring the load situation in critical points of interest in the bogie frame. Since a field load spectrum of high-fidelity is central to determine the service life or kilometers on the road of a component, an assembly, or the whole system, many researches are devoted to standardized methods for load spectrum for critical components like bogie frames of HSTs [15,16] and metro vehicles [17]. Ideally, it is much-needed to have the load spectrum of a component or an assembly during its full-life cycle for accurate damage and fatigue life assessment. Due to the steep cost of full-life monitoring, we usually describe the load spectrum based on limited data from field tests [18], and then extend it to the full-life cycle. Therefore, it is essential to improve the accuracy of

* Corresponding authors.
E-mail addresses: qli3@bjtu.edu.cn (Q. Li), yujie_wei@lnm.imech.ac.cn (Y. Wei).

https://doi.org/10.1016/j.ijfatigue.2021.106221
Received 11 November 2020; Received in revised form 20 February 2021; Accepted 23 February 2021
Available online 8 March 2021

load spectrum from limited experimental data.

For fatigue-sound design, the parametric extrapolation (PE) and nonparametric extrapolation (NPE) are commonly used methods for load spectrum extrapolation [19]. The PE [20,21] method is computationally efficient, but needs a distribution of the load spectrum as a prior. The NPE, on the other hand, relies more on the data than its distribution. For instance, Wu et al. [22] use the Kernel density estimation (KDE) method to extrapolate the dynamic stress on the gearbox with a total running distance of 140,000 km and then to estimate its fatigue damage. More recently, the diffusion-based kernel density estimation (DKDE) [23] is developed to approximate the load spectra of bogie frames. Deep learning method may also provide an alternative to extrapolate load spectrum by using sequence learning to establish a mapping between available information and likely incomplete known physical quantities [24]. Based on discrete wavelet transform and improved deep belief network, Zou et al. [25] propose a new fault diagnosis method for the bearing of traction motor. Related research proves that machine learning method has a broad prospect in the field of fatigue engineering.

In this paper, we focus on the bogie frame of the Chinese Electric Multiple Units (EMUs), and conduct long-term field tests to monitor the stress-time histories in critical points of fatigue. It is revealed that the stress spectra, achieved using rainflow counting method based on field tests for various operating routes and dates, show segmented characteristics with increasing steps of classifications. We propose a high-fidelity approximation for the load spectrum of the bogie frame in a HST by utilizing segmented Weibull distribution (S-Weibull). Such a treatment improves the accuracy of load description and hence realize better results on cumulative damage evaluation. More importantly, we revealed a critical parameter, the inflection stress, whose magnitude can be employed to assess line quality. It is of significance as the relationship between dynamic loads and line quality, while strongly coupled, receives less attention as no mechanical parameters can be adopted to infer one from another.

2. Field tests and data processing

2.1. Field tests

We have conducted long-term field tests on Beijing ~ Guangzhou (BG), Beijing ~ Shanghai (BS), Beijing ~ Chengdu (BC) and Beijing ~ Taiyuan (BT) passenger dedicated lines (PDLs, as shown in Fig. 1) based on the Chinese EMUs platform from May 2013 to July 2015. These specific PDLs cover most regions in the eastern, the central and the southwestern China. Our tests also ran for an operating mileage of more than 1,000,000 km, to cover complex route environments. Furthermore, data were acquired from the train operating at two speeds, 200 km/h from Wuhan ~ Chengdu of the BC PDL and Shijiazhuang ~ Taiyuan of BT PDL with ballast track, and the train ran at 300 km/h on all other lines with ballastless track.

In this work, we focus on the stresses in potentially high stress sites in the bogie frame. Deformation in those sites were acquired by employing the strain gauge technique [26]. In Fig. 2(a), we show the projected views of the motor bogie frame under investigation, and deformation in 15 points vulnerable to fatigue fracture are measured. The specific positions of those sites in the bogie frame are explained in Table 1. The deformation histories are collected by using the Somat eDAQ data acquisition system [27] (DAQ: data acquisition system). To ensure the authenticity of acquired data, we set the sampling frequency to 500 Hz, which is about 10 times higher than potentially activated natural frequencies of the 15 points. According to the test method in reference [28–30], we implement more specific operations, such as the selection of stress measurement points, the installation of test equipment and the derivation of load stress transfer matrix, etc., which are not to be repeated here.

Fig. 1. Illustration to show the four passenger dedicated lines (PDLs) of the Chinese EMUs for field tests, including Beijing ~ Guangzhou (BG), Beijing ~ Shanghai (BS), Beijing ~ Chengdu (BC), and Beijing ~ Taiyuan (BT).

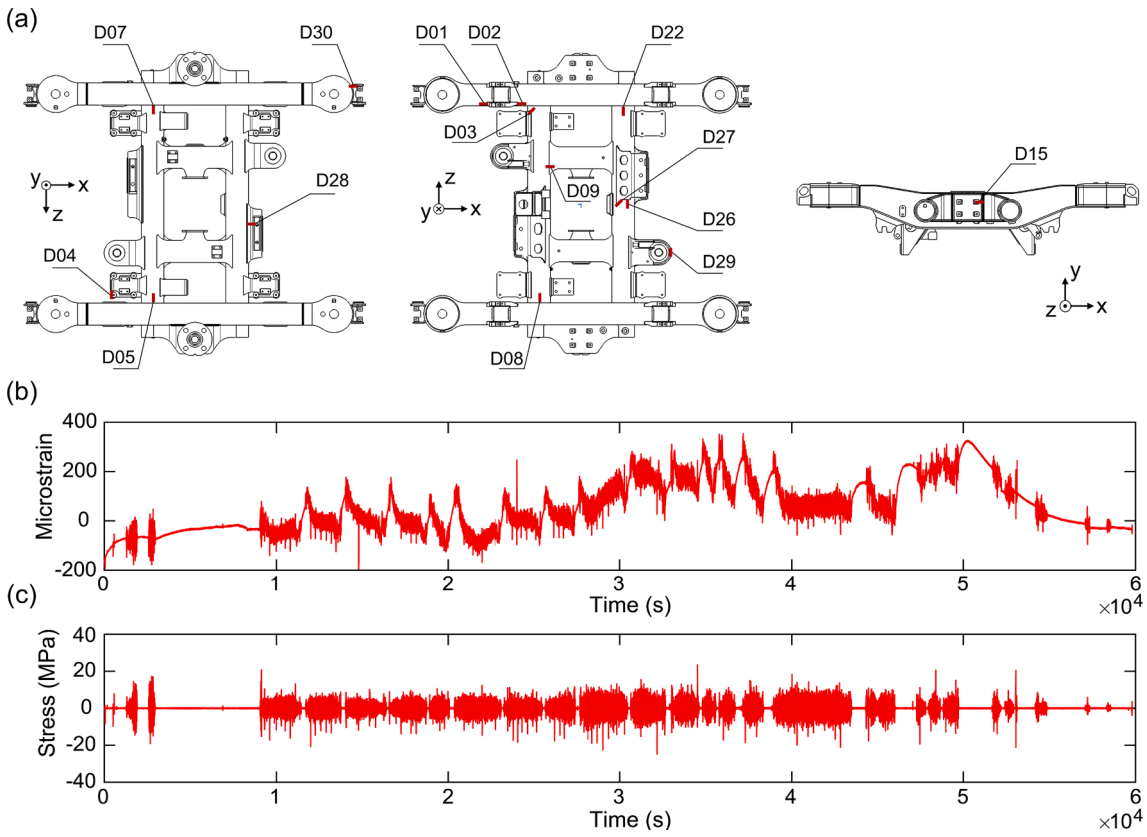

Fig. 2. Field tests setup and data acquisition. (a) The projected views of the motor bogie frame under investigation and the arrangement of strain gauges. (b) Typical signal history of as-received microstrains at point D22, (c) The raw data from (b) were then processed to extract the stress history for spectrum compilation at D22.

Table 1
Descriptions of those points in the motor bogie frame, which are of our interest and their deformation was acquired using strain gauges.

Points (see Fig. 2 (a))	Description
D01 D02	Junction of the side frame and the positioning seat
D03	Junction of the transverse beam and the brake lifting socket
D04	Root of the side bracket of the brake lifting socket
D05 D07	Top of the junction of the transverse beam and the side frame
D08 D22	Bottom of the junction of the transverse beam and the side frame
D09	Junction of the transverse beam and the longitudinal beam
D15	Junction of the side frame and the anti-yaw damper seat
D26 D27	Root of the traction motor lifting socket
D28	Junction of the transverse beam and the traction motor seat
D29	Root of the gearbox lifting socket
D30	Root of the vertical damper lifting socket

2.2. Data processing

Due to possible interferences from many factors, like data drifting caused by temperature variation, periodic electromagnetic signals, and abnormal stress peaks induced by self-vibration of testing equipment, and so forth, the acquired raw data should be processed before used for further analysis:

(1) Zero drift removal. Observe the initial signals of measured points within time domain, and determine the effective starting and ending time for each section of signals in combination with the operating timetable of the HST. Check whether there are zero drifts involved in the signals, and remove them if any;
(2) Signal de-noising. Eliminate noisy signals generated by the equipment such as power-line interference through digital filtering, and remove abnormal signals induced by possible external random disturbances;
(3) Signal conversion. Convert the original strain signals into stress or force signals according to the inherent conversion law between physical quantities.

After following the protocols shown above, raw microstrain histories acquired from field tests, as seen in Fig. 2(b), are transformed to stress sequences given in Fig. 2(c), which are then compiled into a load spectrum for fatigue analysis later on.

3. Segmented characteristic of load spectrum

3.1. Compiling load spectrum

After data processing, we adopt the rainflow counting method [31] to convert the load-time history to rainflow matrix, and then construct a load spectrum by utilizing different classifying methods. Unless stated otherwise, we use even classification in what follows. Some simplified

methods may be adopted when constructing the load spectrum. For example, the cycles of small loads in a load spectrum often accounts for a predominant portion of the total cycles. There are many small-load-omitting criteria (SLOC) [32] for a variety of engineering structures, such as criteria based on the percentage of the maximum load amplitude [33] or the fatigue limit for materials [34]. It is noted that the fatigue damages of different structures or materials under small load amplitudes are quite different, and the high-frequency small loads often have a perceivable contribution to the damage in some components of HSTs. As detained in Section 4.2, it is meaningful to retain the high-frequency small load amplitude part from the original load spectrum, in order to obtain the holistic characteristics of a load spectrum. In addition, the load spectrum is simplified and represented by a small number of steps, with which engineers may perform indoor fatigue tests at each load step. For instance, 64-step classification is recommended in accordance with the European standard [35] when compiling the load spectrum of a bogie frame. Such a procedure, while broadly implemented in engineering practice, brings up possible inconsistency between damages induced by a real load spectrum and those using a coarse-step representation.

With the availability of a vast amount of data and increasing computation power, it is of significance to first find the most accurate representation of a load spectrum, and come up with an accurate yet simple fitting method of the load spectrum. In the following, we provide several classifying methods and compare their accuracies in damage assessment, and try to propose a better description of the load spectrum.

3.2. The steps of classifications

A typical load spectrum contains innumerable loads of distinct magnitudes which may repeat at different frequencies. The process of classification is to determine how many steps of stress and at what frequency, in order to simplify the damage assessment about the load spectrum. As a prerequisite, we need to define the span of load amplitude from a rainflow matrix, which is the difference of the maximum and the minimum amplitude. In practice, the minimum amplitude is set to zero by default, unless a small-load-omitting criterion is applied. The load span is then divided into multiple steps, and the times related to the occurrence at each stress amplitude are the cumulative frequency of stresses falling into the stress interval. For a combined consideration over efficiency and accuracy, there are five commonly used classifications [3,35–39] of load spectra, which are now broadly used and are briefly summarized in following.

(i) Eight-step even classification: The eight stress amplitudes within a load span are evenly spaced [36,37];
(ii) Eight-step non-even classification: The eight stress intervals are determined from an ad hoc load histogram, and are given as a fraction of the maximum stress amplitude, {0.125, 0.15, 0.15, 0.15, 0.15, 0.125, 0.10, 0.05}, from low to high stress, in turn [3];
(iii) 64-step even classification: The 64 stress amplitudes within a load span are evenly spaced [35];
(iv) Optimal multi-step even classification: Stress steps are obtained using equal intervals, and the optimal interval is determined by the Sturges formula [38]:

$$C = \frac{R}{1 + 3.322(lgN)} \tag{1}$$

where N is the number of load cycles or the total frequency of loads with distinct amplitude, and R is the load span. For a load spectrum composed of 1,000,000 distinct load amplitudes, roughly we need 21 steps.

(v) Minimum multi-step even classification: Equal stress interval is adopted in this type of classification, and a minimum number of steps is required. The minimum step number is suggested by Terrell and Scott [39] as follows:

$$S_t \geq \sqrt[3]{2N} \tag{2}$$

For $N = 1,000,000$, the desired number of steps is no less than 126.

Bear in mind the selection on steps in aforementioned classifications is contingent on (1) an accurate representation of a particular load spectrum and (2) the need to duplicate fatigue effects through program suitable for laboratory execution [4,37]. It by no means suggests the existence of a best or an optimal strategy in classification. Indeed, if it exists, it should be the real load spectrum we obtain from field tests.

We focus on the welded joint located at the bottom of the junction of a transverse beam and a side frame of the bogie frame, D22 in Fig. 2(a). The stress-time histories in this point while the train ran on BG, BT, BS and BC PDLs were collected. Each data set includes data in more than 12 h. Using the rainflow counting algorithm, we obtain the load spectra from the four PDLs for a chosen classification.

With known stress steps and their frequencies of a load spectrum, we may proceed to calculate the damage D based on the empirical Miner's linear cumulative damage law [40]:

$$D = \sum_{i=1}^{S} \frac{n_i \sigma_i^m}{C} \tag{3}$$

where S is the total number of stress steps, $\{\sigma_1, \cdots, \sigma_i, \cdots, \sigma_S\}$ are the stress amplitudes after classification, n_i stands for the frequency of the i-th step, m is the slope of S-N curve. Here we take welded steel joint as a model case. The welded joint may endure about 2 million cycles under a stress amplitude of 70 MPa and has a reliability of 99%, with$m = 3.5$ and $C = 5.74 \times 10^{12}$ [41–43]. We used the elementary Miner's rule to calculate damage accumulation, in which the amplitude of the component fatigue limit is constant by default, and the fatigue damage is not affected by the loading sequence of different stress step. For more sophisticated derivatives of the Miner's rule, the reader is referred to ref. [44].

As a comparison, we construct the load spectra using the five types of classifying methods. The corresponding damage, obtained from eqn. (3) for the five classifications of load spectra, are D_1 to D_5, respectively. As a comparison, we also calculate the damage D_0 of the point using the original rainflow matrix without classification. We show in Table 2 the absolute value of relative errors of damages E_i resulted from the five types of classifications, and $E_i = \frac{|D_i - D_0|}{D_0}, (i = 1, 2, \cdots, 5)$.

As seen in Table 2, the BS PDL has the better operating condition, while that of the BC PDL is the worst, in consistent with the actual situation of those PDLs given the variant geography [12]. The damages calculated based on load spectra from the five classifying methods are quite different. Method (v) can produce load spectrum with an acceptable damage error as compared with D_0, which could be considered as the actual damage. Note classifying method (iii) leads to an error on the order of 1%. Moreover, Table 2 indicates that when the stress interval is equal, damage error decreases with the increase of steps. Hence, in the absence of a better classifying method, we may ameliorate the accuracy of the obtained load spectrum by increasing the steps of a classification.

Table 2
Errors of calculated damages in D22 of a bogie frame based on load spectra from different classifying approaches compared with the reference one $D_0\left(\times 10^{-9}/\mathrm{km}\right)$. Here S_s and S_t are numbers of steps acquired by method (iv) and (v), respectively.

Railway	Date	D_0	E_1(%)	E_2(%)	E_3(%)	E_4(%)	S_s	E_5(%)	S_t
BG PDL	13.05.25	**1.239**	173.6	85.30	0.8258	7.271	24	0.05045	243
BT PDL	13.05.03	**1.196**	372.2	167.5	1.389	13.30	24	0.06094	259
BS PDL	14.10.23	**0.6297**	384.7	154.4	1.503	17.09	22	0.1467	169
BC PDL	15.03.30	**2.093**	155.0	86.64	0.7185	6.485	24	0.06316	241

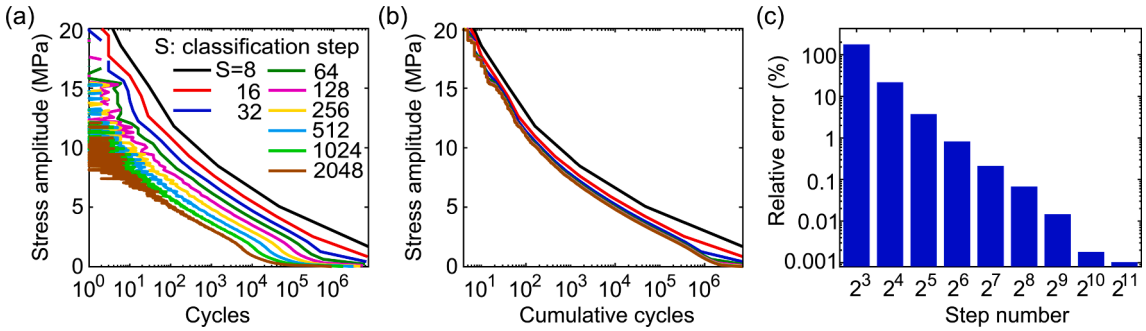

Fig. 3. Stress spectra from D22 of the motor bogie frame. (a) Stress spectra compiled from different steps of a classification with equal intervals, the raw data came from a one-way operation on BG PDL on May 25, 2013. (b) Cumulative cycles diagram of spectra with different steps corresponding to (a). (c) The dependence of relative errors of damages on classifying steps. Note a classification with S = 64 leading to a relative error less than 1%.

We emphasize that cautions should be exercised when compiling similar stress spectrum. To make the damage induced by the compiled load spectrum close to the reality, high-frequency small loads may have to be retained, and the steps of a classification should be sufficiently large.

3.3. The segmented characteristic

Here, we take the stress-time history in D22 measured from one-way operation on BG PDL as an example and demonstrate in Fig. 3(a) to (c) the effect of classifying steps on the pattern and accuracy of the obtained load spectrum, respectively. As seen in Fig. 3(c), increasing steps of a classification may give rise to a prominent reduction in relative errors in damages. In particular, 64-step classification could lead to a relative error less than 1% while the damage from a load spectrum of 2048-step classification is fully consistent with the actual one. More importantly, Fig. 3(a) shows that with increasing steps of a classification, the stress spectrum gradually exhibits a significantly segmented characteristic. There is an inflection point near the location of 10% of the maximum amplitude, where the slope of the stress-frequency curve changes abruptly. We define the stress amplitude at the abrupt slope change point as the inflection stress. Fig. 3(b) shows stress vs. cumulative cycles, and we see that the difference resulted from the choice of steps is still considerable. It therefore suggests that the damage difference caused by different steps is not an artefact. Only when the number of steps reaches a certain amount, the stress spectra of different steps converges. Note that a large step number is desired to reveal such an intrinsic segmented characteristic of the stress spectrum, which may explain why the feature is missing in previous studies [16,18].

We now aim to examine the generality of the segmented feature and explore its origin. Since we have removed the noise of DAQ from experiment data in Section 2.2, the segmented feature may come from noise of the frame itself or from external loads. Dynamics simulations may help us to identify the origin of the segmented feature (see the Appendix). By using the external forces as the inputs in the simulation, the outcome force spectra from our dynamics simulations are also segmented, as shown in Fig. S2. We therefore conclude that the external loads are the cause of such a feature.

To illustrate the generality of the segmented characteristic of those load spectra, we explore the load spectra obtained from the same site D22 on distinct operating lines and at different time. Firstly, we select the representative one-day stress-time histories in D22 of the bogie frame for a motor car from four PDLs. A 2048-step classification is

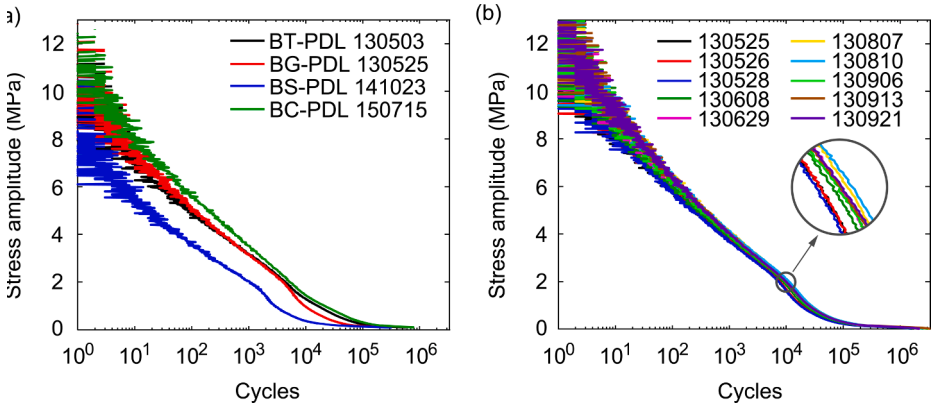

Fig. 4. The influence of lines and time on stress spectrum. The stress spectra in D22 of the bogie frame for a motor car: (a) Stress spectra from BT, BG, BS and BC PDLs from a one-day operation; (b) Stress spectra from BG PDL on different dates.

adopted, and the stress spectra from the four PDLs are shown in Fig. 4(a). The stress spectra from different PDLs exhibit similar segmented characteristics.

The data from the BG PDL are used to evaluate the influence of operating date on load spectrum. Fig. 4(b) shows the stress spectra compiled from data obtained on different dates, and each spectrum is a representation of data from a one-day operation on the BG PDL. We see all stress spectra exhibit very similar segmented characteristics and their distributions are almost the same, indicating that the characteristic of load spectra from a certain PDL remains stable. Therefore, the segmented nature of the stress spectra seems to be independent on routes and operating time.

4. Segmented Weibull distribution

The segmented nature of the stress spectrum is not readily captured by existing distributions. We introduce in this part a segmented Weibull distribution (S-Weibull) to describe the stress spectrum from large steps of a classification, and explore the significance of parameters of the S-Weibull model.

4.1. Method description

The Weibull distribution, like lognormal distribution, is a commonly used hypothesis distribution that is widely applied in cumulative failure problems of mechanical and electrical products. The three-parameter Weibull distribution (3-Weibull) method, a classical parametric estimation method considering the influences of both mean value and amplitude of data, is the most widely used in fitting the load spectrum of bearing components of HSTs [21].

The cumulative distribution function (CDF) and probability density function (PDF) of a typical 3-Weibull are defined as

$$F_3(x) = 1 - \exp\left[-\left(\frac{x-\gamma}{\eta}\right)^{\beta}\right], x \geq \gamma \tag{4}$$

$$f_3(x) = \frac{\beta}{\eta}\left(\frac{x-\gamma}{\eta}\right)^{\beta-1}\exp\left[-\left(\frac{x-\gamma}{\eta}\right)^{\beta}\right], x \geq \gamma \tag{5}$$

where the position parameter $\gamma \geq 0$, η and β are positive scale parameter and shape parameter, respectively. When $\gamma = 0$, it degenerates into a two-parameter Weibull distribution (2-Weibull) model [45].

Nevertheless, the fitting accuracy of 3-Weibull approach is not high enough in practical applications [18], let alone matching the segmented characteristic of load spectrum found in this paper. In addition to the conventional parametric estimation methods, some nonparametric estimation approaches such as kernel density estimation (KDE) algorithm have been developed to achieve the high-precision fitting of load spectrum [22]. However, the KDE method relies heavily on the selection of kernel function and bandwidth, and is much inefficient compared with parametric estimation methods. Here, we propose a novel segmented Weibull distribution (S-Weibull) method to fit the segmented characteristic of load spectrum, which uses a piecewise function to fit the probability density of the stress spectrum before and after the inflection point, aiming to not only retain the efficiency and engineering practicability of the parametric estimation method, but also achieve an accuracy comparable to that of the nonparametric estimation approach.

The specific form of segmented Weibull distribution is as follows: the segment before the inflection point is a superposition of two 2-Weibull, while that after the inflection point is a 3-Weibull. Hence, the PDF of S-Weibull could be readily written as

$$f_s(x) = \begin{cases} \frac{\beta_1}{\eta_1}\left(\frac{x}{\eta_1}\right)^{\beta_1-1}\exp\left[-\left(\frac{x}{\eta_1}\right)^{\beta_1}\right] + \frac{\beta_2}{\eta_2}\left(\frac{x}{\eta_2}\right)^{\beta_2-1}\exp\left[-\left(\frac{x}{\eta_2}\right)^{\beta_2}\right], & 0 < x < \sigma_0 \quad (6a) \\ \frac{\beta_3}{\eta_3}\left(\frac{x-\gamma_3}{\eta_3}\right)^{\beta_3-1}\exp\left[-\left(\frac{x-\gamma_3}{\eta_3}\right)^{\beta_3}\right], & x \geq \sigma_0 \quad (6b) \end{cases}$$

The CDF can be obtained by integration as

$$F_s(x) = \begin{cases} 2 - \exp\left[-\left(\frac{x}{\eta_1}\right)^{\beta_1}\right] - \exp\left[-\left(\frac{x}{\eta_2}\right)^{\beta_2}\right], & 0 < x < \sigma_0 \quad (7a) \\ 2 - \exp\left[-\left(\frac{\sigma_0}{\eta_1}\right)^{\beta_1}\right] - \exp\left[-\left(\frac{\sigma_0}{\eta_2}\right)^{\beta_2}\right] + \exp\left[-\left(\frac{\sigma_0-\gamma_3}{\eta_3}\right)^{\beta_3}\right] - \exp\left[-\left(\frac{x-\gamma_3}{\eta_3}\right)^{\beta_3}\right], & x \geq \sigma_0 \quad (7b) \end{cases}$$

where σ_0 is the inflection stress. Note that the PDF and CDF of the two segments of the S-Weibull should meet the C_0-continuity at the inflection point.

The steps of our fitting procedures are as follows: (1) We convert the measured load spectrum into the probability density distribution of load amplitudes; (2) The proposed S-Weibull is adopted to fit the converted probability density distribution of load amplitudes, and its parameters are optimized through the trust-region algorithm to minimize the root mean squared error (RMSE) of the fitting results; (3) We normalize the fitted S-Weibull to a distribution function with a cumulative probability of 1, and then use it to deduce a fitted load spectrum with the same cumulative cycles as the original one. Fig. 5 shows the detailed

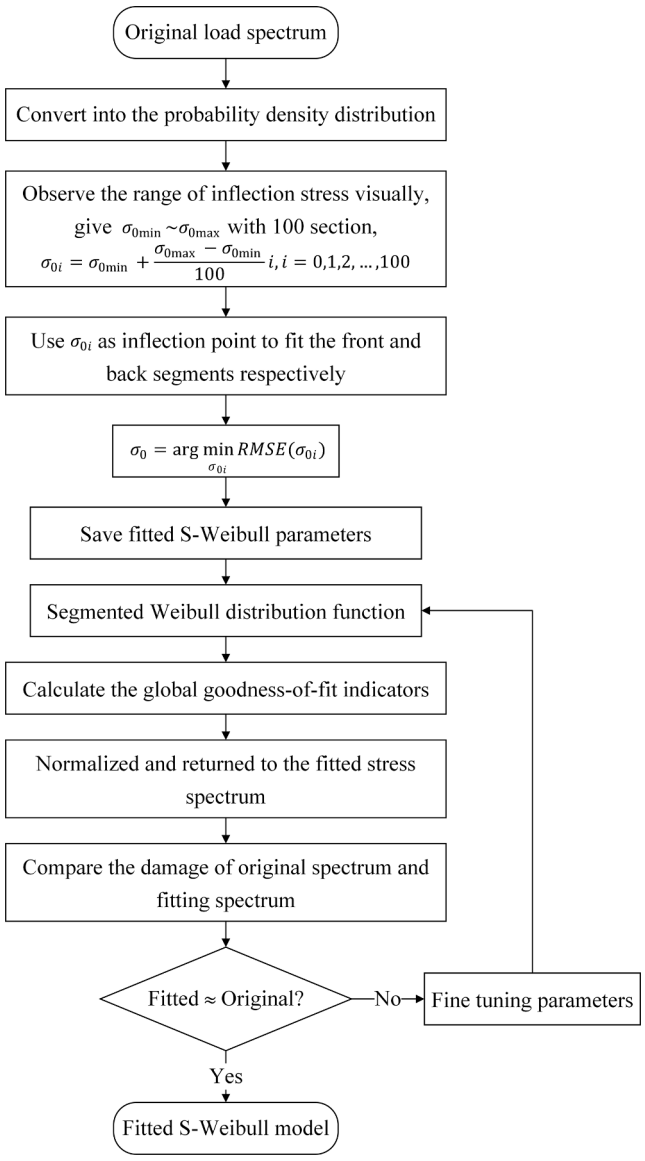

Fig. 5. Execution process to fit the load spectrum by using the S-Weibull method.

execution process to fit the load spectrum. Noted that when the damages of the original spectrum and the fitted spectrum are compared at the end, in order to make the two consistent, the fine-tuning parameters will not affect the distribution of the S-Weibull function, and only slightly change the goodness-of-fit indicators.

We extracted two days of measured deformation in D22 for each of the four PDLs, and the stress spectra are then fitted by using the S-Weibull, as shown in Fig. 6. The inflection stress σ_0 of the fitted spectra are also indicated in each subgraph. The parameters of the PDF of S-Weibull are shown in Table 3. The agreement between the fitted probability densities of stress spectra and the original ones for all four PDLs is reasonable. In particular, the results demonstrate that our S-Weibull method is able to accurately describe the observed segmented characteristic of load spectrum and is appliable to multiple PDLs.

4.2. Accuracy validation

We also use the 3-Weibull approach and Gaussian-KDE algorithm to approximate the eight stress spectra shown in Fig. 6, respectively, and further compare the accuracy of our S-Weibull fitting approach with the two methods. The bandwidth of Gaussian-KDE is set to 0.15. In terms of fitting efficiency, regardless of the development time of fitting program, the running time of S-Weibull program is similar to that of KDE. The difference is that the former needs only one fitting, while the latter needs to manually set parameters including the kernel function and the bandwidth.

Here, three goodness-of-fit indicators, namely RMSE, coefficient of determination (R^2) and Kolmogorov-Smirnov (KS) test statistic, are employed to evaluate the accuracy of different methods in approximating the probability density. The formulations of the three goodness-of-fit indicators are defined as

$$RMSE = \sqrt{\frac{1}{S}\sum_{i=1}^{S}\left(y_i - \widehat{y}_i\right)^2} \tag{8}$$

$$R^2 = \frac{\sum_{i=1}^{S}\left(\widehat{y}_i - \overline{y}\right)^2}{\sum_{i=1}^{S}\left(y_i - \overline{y}\right)^2} \tag{9}$$

$$KS = \sup_i \left|P(i) - \widehat{P}(i)\right| \tag{10}$$

where S is the total number of stress steps, y_i and $\widehat{y}_i$ are original and fitted probability densities of the i-th step, respectively; $\overline{y}$ is the mean value of original probability densities, $P(i)$ and $\widehat{P}(i)$ are original and fitted cumulative probability densities of the i-th step, respectively.

As seen in Table 4, the S-Weibull method has the highest approximate accuracy of all indicators among the three approaches, of which the RMSE is about 0.5%. This is comparable to the recently developed diffusion-based kernel density estimation (DKDE) algorithm [23] in approximate precision, while is more efficient and easier to conduct. Therefore, our method can not only achieve the same efficiency as the common parameter estimation methods [21], but also surpass the previous two methods in accuracy.

We still take the stress spectrum in D22 measured from a one-way operation on BG PDL as an example, and demonstrate in Fig. 7(a) the original stress spectrum from tests and the corresponding approximate ones obtained using the above three methods. It can be seen that the 3-Weibull approach has the worst ability in approximating the small stress and stresses near the inflection point. In contrast, both the S-Weibull method and Gaussian-KDE algorithm can effectively describe the segmented feature of stress spectrum, and show similar accuracy over the entire stress amplitude range except that the former is superior to the later in terms of approximate accuracy for small stress amplitude. In Fig. 7(b), we show the induced damages at each step of the four spectra in Fig. 7(a). As seen in Fig. 7(b), the 3-Weibull approach has the worst fitting accuracy for damage at each step, while both S-Weibull fitting method and Gaussian-KDE algorithm keep high-fidelity.

In Table 5, we further present the comparison between the damages calculated from the eight measured stress spectra depicted in Fig. 6 and those produced by the approximate stress spectra obtained using the 3-Weibull approach, Gaussian-KDE algorithm and S-Weibull method. From the perspective of cumulative damages, the S-Weibull method is the most superb. Note that the damage of the load spectrum obtained

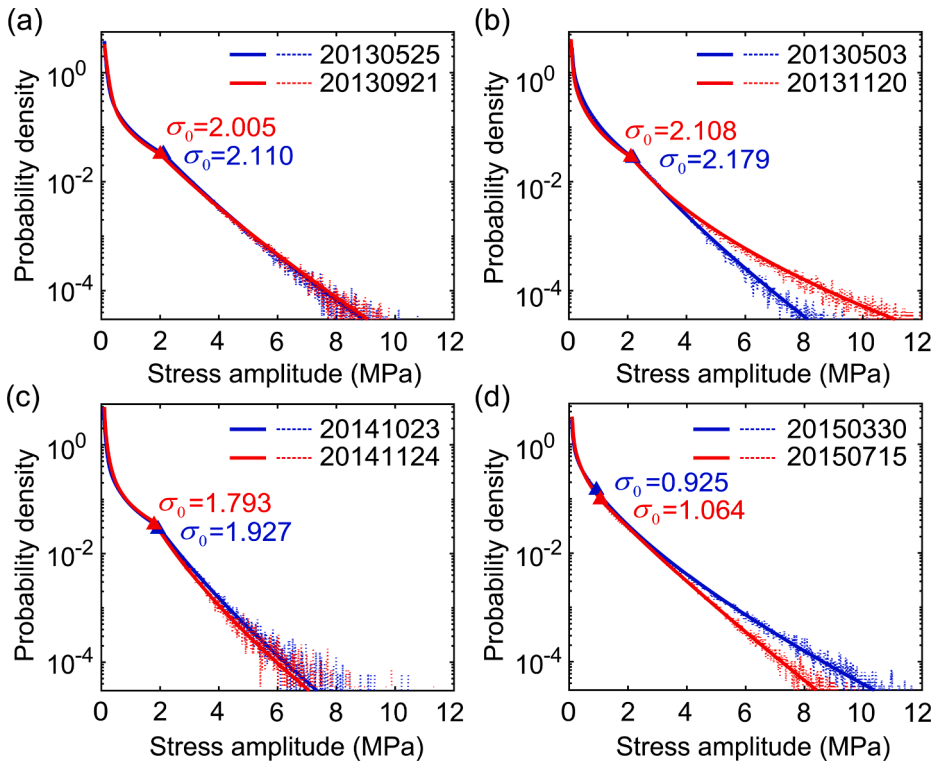

Fig. 6. Comparisons between probability densities of stress spectra in D22 from tests (dashed lines) and those using the S-Weibull method (solid lines). Here, we arbitrarily extract data within two days of operation from (a) BG PDL, (b) BT PDL, (c) BS PDL and (d) BC PDL, respectively.

Table 3
Parameters of the segmented Weibull distribution fitted by each stress spectrum in Fig. 6.

Railway	Date	η_1	β_1	η_2	β_2	σ_0	η_3	β_3	γ_3
BG PDL	13.05.25	0.283	0.326	0.104	0.996	**2.110**	0.870	0.766	−0.357
BG PDL	13.09.21	0.285	0.313	0.135	0.909	**2.005**	0.930	0.769	−0.644
BT PDL	13.05.03	0.380	0.486	0.076	1.189	**2.179**	0.650	0.728	0.175
BT PDL	13.11.20	0.290	0.389	0.059	1.013	**2.108**	0.204	0.487	1.298
BS PDL	14.10.23	0.200	0.291	0.072	0.911	**1.927**	0.549	0.717	0.270
BS PDL	14.11.24	0.181	0.197	0.085	1.027	**1.793**	0.283	0.617	0.524
BC PDL	15.03.30	0.685	0.470	0.055	0.995	**0.925**	0.753	0.685	−0.334
BC PDL	15.07.15	0.321	0.442	0.075	1.184	**1.064**	1.230	0.868	−1.517

using our S-Weibull approach could achieve the consistency with the real one by fine-tuning parameters of the PDF, which suggests the flexibility and efficiency of the method. Moreover, the damages evaluated from the eight measured stress spectra removing the small stress parts less than 5% and 10% of the maximum stress amplitude, which are lower than the common small-load-omitting levels applied in most researches [32,33], are also added to the comparison in Table 5. It can be seen that the small amplitude part of a load spectrum has a non-ignorable contribution to the cumulative damage of structures, and hence we should retain such part cautiously during the load spectrum compilation and fitting process to meet the desired accuracy for the subsequent damage assessment.

4.3. *Inflection stress and its relationship with line quality*

To investigate the influence of line conditions on the value of in-

Table 4
Comparison for goodness-of-fit of different approximation methods. Here, 3-W, G-KDE and S-W stand for 3-Weibull approach, Gaussian-KDE algorithm and S-Weibull method, respectively.

Railway	Date	RMSE			R^2			KS test statistic		
		3-W	G-KDE	S-W	3-W	G-KDE	S-W	3-W	G-KDE	S-W
BG PDL	13.05.25	0.0850	0.0804	0.0032	0.9405	0.9467	0.9999	0.2128	0.1661	0.0041
BG PDL	13.09.21	0.0747	0.0669	0.0029	0.9282	0.9423	0.9999	0.2276	0.1505	0.0046
BT PDL	13.05.03	0.0120	0.0536	0.0047	0.9983	0.9663	0.9997	0.0381	0.1179	0.0189
BT PDL	13.11.20	0.0227	0.0730	0.0064	0.9938	0.9361	0.9995	0.1181	0.1654	0.0236
BS PDL	14.10.23	0.0806	0.0987	0.0037	0.9577	0.9364	0.9999	0.1822	0.1988	0.0023
BS PDL	14.11.24	0.0759	0.1019	0.0015	0.9915	0.9847	0.9999	0.1437	0.1889	0.0016
BC PDL	15.03.30	0.0357	0.0548	0.0041	0.9815	0.9565	0.9998	0.0735	0.1164	0.0133
BC PDL	15.07.15	0.0572	0.0602	0.0025	0.9707	0.9675	0.9999	0.1698	0.1335	0.0106

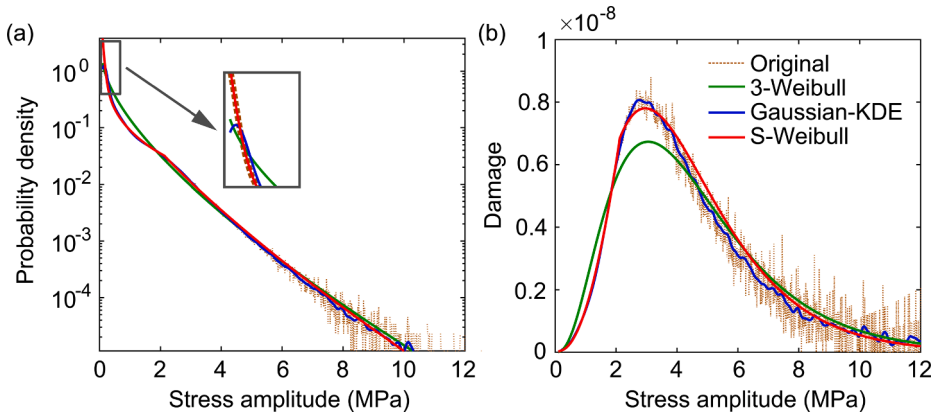

Fig. 7. Comparisons of (a) probability densities of stress spectra and (b) damages at each step from tests and those obtained using different methods. The raw data used here were obtained from a one-way operation on BG PDL on May 25, 2013.

flection stress, we focus on the BG and BC PDLs. In practice, the BG PDL is divided into six sections: in turn are Beijing ~ Shijiazhuang (A_{gc}), Shijiazhuang (A_{gc}) ~ Zhengzhou (B_{gc}), Zhengzhou (B_{gc}) ~ Wuhan, Wuhan ~ Changsha (C_g), Changsha (C_g) ~ Chenzhou (D_g), and Chenzhou (D_g) ~ Guangzhou as illustrated in Fig. 1. The same three sections are applied between Beijing and Wuhan of BC PDL, which are shared with the BG PDL. The rest of the BC PDL is divided into five sections: from East to West are Wuhan ~ Qianjiang (C_c), Qianjiang (C_c) ~ Yichang (D_c), Yichang (D_c) ~ Jianshi (E_c), Jianshi (E_c) ~ Chongqing (F_c) and Chongqing (F_c) ~ Chengdu as marked in Fig. 1. Then, we adopt the proposed S-Weibull method to fit the stress spectra in D22 of the bogie frame, derived from the above 14 sections of both PDLs on distinct operating dates (as indicated in Fig. 8(a)). We show in Fig. 8(a) the inflection stress of the fitted stress spectrum from each operating section on different dates, where the RMSE of fitting for each stress spectrum is within 0.0012 and 0.0064. Note that the track of Wuhan ~ Chengdu section is ballast track, and the running speed of HST is 200 km/h.

We could see from Fig. 8(a) the obvious difference between the locations of inflection stress for fitted stress spectra from distinct operating sections. The inflection stress from BG PDL is significantly greater than that from BC PDL since they separate from Wuhan. With the basic consistency between those from the shared sections of the two PDLs, all the inflection stresses of stress spectra roughly fall within an interval between 1.8 and 2.2 MPa. As observed in Fig. 8(a), the inflection stresses of stress spectra from the same sections are at similar levels, which are generally independent on the operating dates. As the field tests between Wuhan and Guangzhou in the BG PDL were performed on ballastless tracks at an operating speed of 300 km/h while those from Wuhan to Chengdu in the BC PDL were conducted on ballast tracks with a running speed of 200 km/h, it is reasonable to draw the conclusion that the distinct route conditions of the PDLs are the major cause of the difference in the inflection stresses.

To examine the correlation between line conditions and their inflection stresses, we analyze the load spectra of four PDLs, a two-day field data was acquired at the same operating speed of 300 km/h and on ballastless tracks. We show in Fig. 8(b) the distribution of inflection stresses and the corresponding damages of the concerned 13 sections, as keyed in the inset on the top of the figure. For better view, we choose the symbol in the figure matches, in both color and shape, with that marked in the line section shown at the top. It could be inferred that the BS PDL has the best route condition with a damage per kilometer less than 4.22×10^{-10} and a smallest dispersion of inflection stresses, while the route condition of sections between Wuhan and Guangzhou of BG PDL is the worst, which leads to the greatest damages and the most scattering data. It suggests the better the line quality is, the smaller the inflection stress is, and consequently the less damage would be. These observations are in consistent with the real conditions of the four routes. The inflection stress may then be used as an indicator to characterize the quality of line conditions.

Table 5

Comparison of calculated damages in D22 of the bogie frame based on stress spectra obtained from different approximation approaches. Here, the original damages D_0 calculated from the eight measured stress spectra shown in Fig. 6 are used as references. $D_{5\%}$ and $D_{10\%}$ are damages obtained from the measured stress spectra removing the small stress amplitude parts less than 5% and 10% of the maximum stress amplitude, respectively. D_{3-W}, D_{G-KDE}, and D_{S-W} in turn are damages calculated from the stress spectra obtained using the 3-Weibull approach, Gaussian-KDE algorithm and S-Weibull method. $E_{5\%}$, $E_{10\%}$, E_{3-W}, E_{G-KDE} and E_{S-W} are the absolute values of their relative errors (%) compared with the references. The unit of damage is 10^{-9}/km.

Railway	Date	D_0	$D_{5\%}$	$E_{5\%}$	$D_{10\%}$	$E_{10\%}$	D_{3-W}	E_{3-W}	D_{G-KDE}	E_{G-KDE}	D_{S-W}	E_{S-W}
BG PDL	13.05.25	**1.239**	1.214	2.053	1.016	18.04	1.210	2.381	1.243	0.3323	1.241	0.1380
BG PDL	13.09.21	**1.290**	1.258	2.465	1.030	20.12	1.250	3.078	1.294	0.3208	1.288	0.1297
BT PDL	13.05.03	**1.196**	1.126	5.811	0.7820	34.60	1.171	2.071	1.201	0.4283	1.197	0.1393
BT PDL	13.11.20	**2.203**	2.110	4.225	1.716	22.11	2.062	6.409	2.208	0.2173	2.201	0.0794
BS PDL	14.10.23	**0.6297**	0.6043	4.034	0.4453	29.30	0.6068	3.640	0.6322	0.3963	0.6296	0.0213
BS PDL	14.11.24	**0.4543**	0.4356	4.118	0.3177	30.08	0.4383	3.530	0.4566	0.5015	0.4541	0.0510
BC PDL	15.03.30	**2.093**	2.034	2.811	1.740	16.85	2.070	1.067	2.098	0.2521	2.094	0.0546
BC PDL	15.07.15	**1.473**	1.396	5.253	1.047	28.92	1.607	9.085	1.477	0.2961	1.475	0.1260

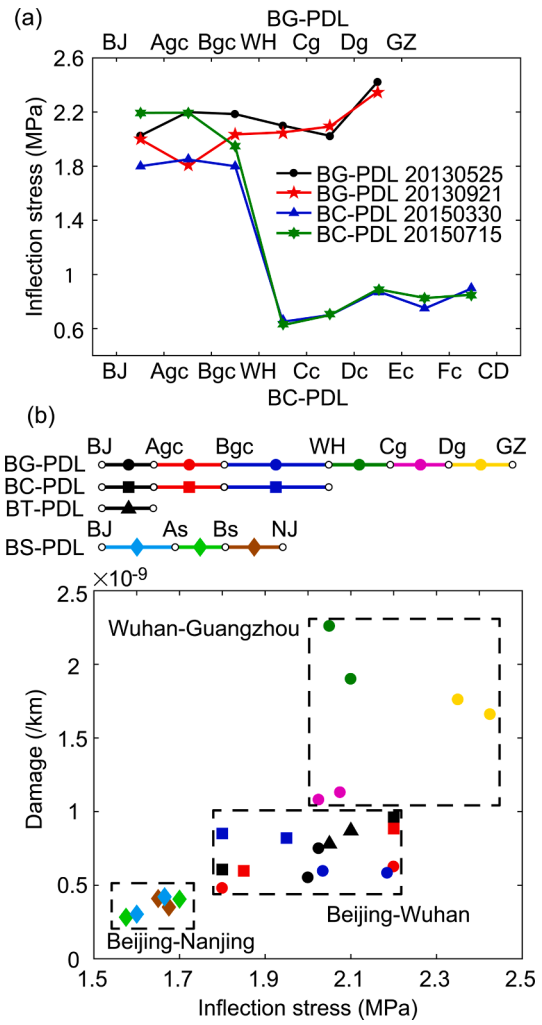

Fig. 8. Influence of line conditions on the inflection stress when using the S-Weibull in order to match the stress spectra at D22 of the bogie frame. (a) Inflection stress distribution of different PDLs with the same section. Here stress spectra from different PDLs and operation dates were used to show their respective influence. Note the inflection stress from BG PDL is significantly higher than that from BC PDL since they split in Wuhan. (b) Correlation between damages incurred by loading spectra in different spans and their inflection stresses. The symbol in the figure matches with that marked in the line section shown at the top. It suggests the better the line quality is, the smaller the inflection stress is, and consequently less damage. Here, BJ, WH, GZ, NJ and CD are abbreviations of Beijing, Wuhan, Guangzhou, Nanjing and Chengdu, respectively.

5. Conclusions

In this paper, we focus on the characterization for actual load spectrum of the bogie frame in a Chinese high-speed train in operation, and find following features associated with the stress spectrum from long-term field tests: (1) With increasing steps of a classification, the load spectra in critical point of a motor bogie frame exhibit an apparent segmented characteristic. Such segmented feature is independent on the operating routes and dates, and is determined by the external loads. (2) A segmented Weibull distribution method is proposed to capture the segmented characteristic of load spectrum, and the S-Weibull shows higher accuracy in terms of cumulative damage evaluation in contrast to other commonly used parametric approximation methods. (3) The inflection stress used in the S-Weibull model may be adopted as an effective indicator of line conditions. The distinct line conditions of the PDLs are the major cause of the difference in the inflection stresses. For ballastless track, the better the line quality is, the smaller inflection stress and consequently the less damage would be.

The directly parameterization for the load spectrum - line quality relationship is hardly seen in existing literature. Although both Beijing ~ Wuhan and Beijing ~ Nanjing sections use the same CRTS II ballastless slab track, due to more curves and tunnels, the damage per kilometer of the bogie frame operating on Beijing ~ Wuhan is higher than that on Beijing ~ Nanjing. The inflection stress captures this feature, which proves that it is not only affected by the track excitation [46], but also a resultant of the comprehensive line environment such as tunnels, bridges, long steep grades and other external factors on the bogie frame of a HST. The S-Weibull method suggested here may provide an alternative description about the load spectrum for high-speed trains and other dynamics systems, and the inflection stress parameter could be meaningful metric for the contribution of environmental factors to a load spectrum.

Declaration of Competing Interest

The authors declare that they have no known competing financial interests or personal relationships that could have appeared to influence the work reported in this paper.

Acknowledgements

The authors acknowledge support from the National Key Research and Development Program of China (2017YFB0202800), the NSFC Basic Science Center for 'Multiscale Problems in Nonlinear Mechanics' (No. 11988102), the Strategic Priority Research Program of the Chinese Academy of Sciences (XDB22020200), and CAS Center for Excellence in Complex System Mechanics.

Appendix A. Dynamic model validation

The intricate interactions between connecting components render the HST a typical complex dynamic system [47]. There are many mature methods for dynamic modeling of HST systems, such as vehicle-track coupling dynamic approach [48], vehicle rigid-flexible coupling dynamic theory [49] and so on. We adopt the SIMPACK software of Dassault Systèmes [50] to develop a multi-body dynamic model for a single car of a HST, as illustrated in Fig. S1. The dynamic model is composed of a car body, two bogie frames, four wheelsets, rail track and several sets of essential elements, and each bogie frame bears four vertical forces and four lateral forces, as keyed in Fig. S1(a) to (c), viewed from the side view, the front view, and the top, respectively. In reality, the primary suspensions between bogie frames and wheelsets are connected through steel springs and axle box rotary arms, while the secondary suspensions between the car body and the bogie frames are linked by air springs. The Kelvin model with an elastic element

and a viscous element in parallel, which provide damping in vertical direction and stiffness in longitudinal, lateral and vertical directions, is employed to model these two types of connections. The equivalent elastic model is adopted to describe the contact forces between wheelsets and rail track. The main parameters involved in the multi-body dynamic model are provided in Table S1. The Maxwell model with an elastic element and a viscous element in series is used to represent the anti-yaw damper between the car body and the bogie frames, where the damping force changes with its velocity, as given in Table S2.

In our model, we match each rigid body with six degrees of freedom: the longitudinal, lateral and vertical displacements, and the roll, yaw and pitch. Therefore, the single car model composed of four wheelsets, two frames and one car body, has a total of 42 degrees of freedom. In practice, the external force–time histories acquired on-the-ground, including four vertical force–time histories and four lateral force–time histories respectively transmitted from the steel spring and rotary arm of bogie frame of a motor car, are used as inputs of the dynamic model. We apply these measured force–time histories to the corresponding positions of our model as shown in Fig. S1, to obtain the response-time histories at positions of interest on bogie frames through numerical integration algorithm with a time step of 0.002 s.

We obtain the outcome longitudinal force of the anti-yaw damper of the front bogie frame, F_{FA}, as marked in Fig. S1, from dynamic simulations. The anti-yaw damper force obtained from field tests is used to validate the dynamic simulation. In Fig. S2(a), we present the calculated longitudinal force spectra with different classifying steps. The corresponding force spectra versus cumulative cycles are demonstrated in Fig. S2(b) to show the differences caused by different classifying steps. It can be seen that with increasing steps of a classification, the outcome force spectra exhibit significantly segmented characteristics, similar to the stress spectra shown in Fig. 3. It can be seen from Fig. S2(c) that the simulated force spectrum of the anti-yaw damper is consistent with that from field tests. It may be safe to draw the conclusion that the segmented feature is not caused by noise interference during field tests, but a resultant of the external loads.

Appendix B. Supplementary material

Supplementary data to this article can be found online at https://doi.org/10.1016/j.ijfatigue.2021.106221.

References

[1] Kim J-H, Jeong M-C, Lee T-H, Lee W-W, Kong J-S. Development of fatigue prediction model for steel bridges based on characteristics of variable stress spectra. Int J Damage Mech 2017;26(7):951–67.
[2] Zhu S-P, Liu Q, Lei Q, Wang Q. Probabilistic fatigue life prediction and reliability assessment of a high pressure turbine disc considering load variations. Int J Damage Mech 2018;27(10):1569–88.
[3] Conover JC, Jaeckel HR, Kippola WJ. Simulation of field loading in fatigue testing. SAE Int 1967;75(1):543–56.
[4] Grubisic V. Determination of load spectra for design and testing. Int J Vehicle Des 1994;15:8–26.
[5] Heuler P, Klatschke H. Generation and use of standardised load spectra and load-time histories. Int J Fatigue 2005;27(8):974–90.
[6] Yu J, Zheng S, Feng J, Zhao L. New methodology for determination of load spectra for the vehicle accelerated durability testing associated with the time correlated fatigue damage analysis method. Int J Auto Tech 2017;18(3):547–60.
[7] Lin SJ, Long W, Tian DQ, Liao JB. A new fatigue damage accumulation model considering loading history and loading sequence based on damage equivalence. Int J Damage Mech 2017;27(5):707–28.
[8] Bao R, Zhang X. Fatigue crack growth behaviour and life prediction for 2324–T39 and 7050–T7451 aluminium alloys under truncated load spectra. Int J Fatigue 2010;32(7):1180–9.
[9] Lu Y, Zheng H, Zeng J, Chen T, Wu P. Fatigue life reliability evaluation in a high-speed train bogie frame using accelerated life and numerical test. Reliab Eng Syst Safe 2019;188:221–32.
[10] Zhang W, Wu P, Wu X, Zeng J. An investigation into structural failures of Chinese high-speed trains. Eng Fail Anal 2006;13(3):427–41.
[11] Lu Y, Xiang P, Dong P, Zhang X, Zeng J. Analysis of the effects of vibration modes on fatigue damage in high-speed train bogie frames. Eng Fail Anal 2018;89:222–41.
[12] Yang GW, Wei YJ, Zhan GL, et al. Research progress on the mechanics of high speed rails. Adv Mech 2015;45:201507.
[13] Lučanin VJ, Simić GŽ, Milković DD, Ćuprić NL, Golubović SD. Calculated and experimental analysis of cause of the appearance of cracks in the running bogie frame of diesel multiple units of Serbian railways. Eng Fail Anal 2010;17(1):236–48.
[14] Miao BR, Luo YX, Qiu YJ, Peng QM, Jiang CY, Yang ZK. Research on multidisciplinary fatigue optimization design method in structural design of high speed train. Proc struct int 2019;22:102–9.
[15] Zhang SG. Study on testing and establishment method for the load spectrum of bogie frame for high-speed trains. Sci China Ser E 2008;51(12):2142–51.
[16] Ji C, Sun S, Li Q, Ren Z, Yang G. Realistic fatigue damage assessment of a high-speed train bogie frame by damage consistency load spectra based on measured field load. Measurement 2020;166:108164. https://doi.org/10.1016/j.measurement.2020.108164.
[17] Wang BJ, Li Q, Ren ZS, Sun SG. Improving the fatigue reliability of metro vehicle bogie frame based on load spectrum. Int J Fatigue 2020;132:105389. https://doi.org/10.1016/j.ijfatigue.2019.105389.
[18] Xue GJ, Li Q, Wang BJ, Pan W, Li K. Estimation of distribution for rail vehicle dynamic stress. Chin J Mech Eng 2013;49(4):102–5.
[19] Wang J, Chen H, Li Y, Wu Y, Zhang Y. A review of the extrapolation method in load spectrum compiling. Stroj Vestn-J Mech E 2016;62(1):60–75.
[20] Nagode M, Fajdiga M. On a new method for prediction of the scatter of loading spectra. Int J Fatigue 1998;20(4):271–7.
[21] Chen DY, Sun SG, Li Q. Study on deduction and extend of high-speed train load spectrum. Chin J Mech Eng 2018;54(10):151–5.
[22] Wu H, Wu P, Li F, Shi H, Xu K. Fatigue analysis of the gearbox housing in high-speed trains under wheel polygonization using a multibody dynamics algorithm. Eng Fail Anal 2019;100:351–64.
[23] Ma S, Sun S, Wang B, Wang N. Estimating load spectra probability distributions of train bogie frames by the diffusion-based kernel density method. Int J Fatigue 2020;132:105352. https://doi.org/10.1016/j.ijfatigue.2019.105352.
[24] Mozaffar M, Bostanabad R, Chen W, Ehmann K, Cao J, Bessa MA. Deep learning predicts path-dependent plasticity. P Natl Acad Sci USA 2019;116(52):26414–20.
[25] Zou Y, Zhang Y, Mao H. Fault diagnosis on the bearing of traction motor in high-speed trains based on deep learning. Alex Eng J 2021;60(1):1209–19. https://doi.org/10.1016/j.aej.2020.10.044.
[26] Yang SX, Lu NS. Gauge factor and stretchability of silicon-on-polymer strain gauges. Sensors 2013;13(7):8577–94.
[27] Somat eDAQ Data Acquisition Systems-URL: https://www.hbm.com/en/7775/edaqxr-edaq-mobile-rugged-data-acquisition-systems.
[28] Urda P, Muñoz S, Aceituno JF, Escalona JL. Wheel-rail contact force measurement using strain gauges and distance lasers on a scaled railway vehicle. Mech Syst Signal Pr 2020;138:106555. https://doi.org/10.1016/j.ymssp.2019.106555.
[29] Guo Z, Xu J, Chen Y, Guo Z, Yu P, Liu Yu, et al. High-sensitive and stretchable resistive strain gauges: Parametric design and DIW fabrication. Compos Struct 2019;223:110955. https://doi.org/10.1016/j.compstruct.2019.110955.
[30] Li Q, Gao Z-H, Xu W-L, Wang K, Liu S, Ran G-F, et al. Experimental research on the dynamic propagation process of mode I cracks in the rock under directional fracture blasting using the strain gauge method. Eng Fract Mech 2020;235:107113. https://doi.org/10.1016/j.engfracmech.2020.107113.
[31] American Society for Testing and Materials. Standard practices for cycle counting in fatigue analysis E1049–85(2017). PA: West Conshohocken; 2017.
[32] Yan JH, Zheng XL, Zhao K. Experimental investigation on the small-load-omitting criterion. Int J Fatigue 2001;23:403–15.
[33] Tian HL, Bao R, Zhang JY, Zheng XL, Fei BJ. Influence of low load truncation level on crack growth for Al 2324–T39 and Al 7050–T7451. Chin J Aeronaut 2009;22(4):401–6.
[34] Heuler P, Seeger T. A criterion for omission of variable amplitude loading histories. Int J Fatigue 1986;8(4):225–30.
[35] German Institute for Standardization e. V.. Railway vehicles 2. Railway applications: wheelsets and bogies DIN-Heft 491/2:2014-01. Berlin; 2014.
[36] Gassner E, Schutz W. Evaluating vital vehicle components by programme fatigue tests. FISITA Congress, London: Ninth International Automobile Technical Congress; 1962.
[37] Gassner E, Schutz W. Assessment of the allowable design stresses and the corresponding fatigue life. Fatigue Des Proced 1969:291–307.
[38] Sturges HA. The choice of a class interval. J Am Stat Assoc 1926;21(153):65–6.
[39] Terrell GR, Scott DW. Oversmoothed nonparametric density estimates. J Am Stat Assoc 1985;80(389):209–14.
[40] Miner MA, Monica S. Calif. Cumulative damage in fatigue. J Appl Mech 1945;12(3):159–64.
[41] Radaj D. Design and analysis of fatigue resistant welded structures. Abington Publishing, England: Woodhead Publishing Ltd; 1990.
[42] Japanese Industrial Standards. Rolling stock-Bogie-General rules for design of bogie frame strength JIS E 4207:2004. Tokyo; 2019.

[43] Japanese Industrial Standards. Test methods of static load for truck frames and truck bolsters of railway rolling stock JIS E 4208:2004. Tokyo; 2019.
[44] German Mechanical Engineering Industry Association (VDMA). FKM-Guideline. Analytical strength assessment of components in mechanical engineering. 7th issue, Frankfurt; 2020.
[45] Nohut S. Three-parameter (3P) weibull distribution for characterization of strength of ceramics showing R-Curve behavior. Ceram Int 2021;47(2):2270–9. https://doi.org/10.1016/j.ceramint.2020.09.067.
[46] Song Yang, Wang Zhiwei, Liu Zhigang, Wang Ruichen. A spatial coupling model to study dynamic performance of pantograph-catenary with vehicle-track excitation. Mech Syst Signal Pr 2021;151:107336. https://doi.org/10.1016/j.ymssp.2020.107336.
[47] Zhai WM, Liu PF, Lin JH, Wang KY. Experimental investigation on vibration behaviour of a CRH train at speed of 350 km/h. Int J Rai Transp 2015;3(1):1–16.
[48] Zhai WM, Wang KY, Cai CB. Fundamentals of vehicle-track coupled dynamics. Vehicle Syst Dyn 2009;47(11):1349–76.
[49] Ren ZS, Xin X, Sun G, Wei X. The effect of gear meshing on the high-speed vehicle dynamics. Vehicle Syst Dyn 2020. https://doi.org/10.1080/00423114.2020.1711955.
[50] SIMPACK. 2018. Vélizy-Villacoublay Cedex, France: Dassault Systèmes SIMULIA; 2018.